Polymer 51 (2010) 3966–3970

Contents lists available at ScienceDirect

Polymer

journal homepage: www.elsevier.com/locate/polymer

A new possibility for microstructural investigation of clay-based polymer nanocomposite by focused ion beam tomography

Suprakas Sinha Ray*

DST/CSIR Nanotechnology Innovation Centre, National Centre for Nano-Structured Materials, Council for Scientific and Industrial Research, Pretoria 0001, South Africa

ARTICLE INFO

Article history:
Received 30 April 2010
Received in revised form
9 June 2010
Accepted 14 June 2010
Available online 19 June 2010

Keywords:
FIB-tomography
Nanocomposite
Microstructure

ABSTRACT

This article describes the focused ion beam (FIB)-tomography as a high-resolution three-dimensional (3D) technique to study the morphology of polymer/clay nanocomposites. To establish the structure–property relationship of such composite material, it is very important to visualize the 3D-structure and distribution of clay particles in the polymer matrix. The sequential two-dimensional sectioning by FIB, followed by imaging of dispersed silicate layers using high-resolution scanning electron microscope, and computer reconstruction can show the degree of dispersion of silicate layers in 3D-space.

1. Introduction

Over the last decade, the incorporation of nanoclay particles into polymer matrices to produce composite materials has attracted a great deal of research attention, both in industry and in academia, because the addition of a relatively small amount (~5 wt%) of clay remarkably improves mechanical and material properties when compared to those for pure polymer or conventional filler-filled composite materials [1–4]. The main reason for these improved properties in polymer/clay composites (PCNs) is the interfacial interactions or bonds between matrix and clay as opposed to conventional composites. In the case of PCNs, the interfacial area is determined by the aspect ratio of the dispersed clay particles as well as the loading level. As the intercalated silicate layers are more nicely dispersed in the polymer matrix, the thickness of the dispersed particles decreases; as a result the aspect ratio and the effect of the clay particles loading on the matrix mechanical properties increases.

To fully understand the observed properties and also to establish the structure–property relationship of PCN materials, it is very important to visualise their three-dimensional (3D) structure and, in particular, the dispersion/distribution of the clay particles within the polymer matrix and the nature of the interfacial interaction between the matrix and the filler.

The morphology of PCN is generally elucidated using X-ray diffraction (XRD) and transmission electron microscopy (TEM) [3,5]. Although XRD allows a direct evidence of the intercalation of the polymer chains into the silicate galleries, however, little can be said about the spatial distribution of the silicate layers or any structural inhomogeneities in the PCN. On the other hand, TEM allows a qualitative understanding of the internal structure, spatial distribution of the various phases, and defect structure through direct visualization [6]. However, this technique has a serious drawback due to the fact that it projects three-dimensional (3D)-body on to two-dimensional (2D) plane. The information along the thickness direction of the sample is only an accumulated one and this actually leads to the wrong conclusion about the degree of dispersion of silicate layers in the polymer matrix. To avoid this confusion and to get accurate information about the dispersion of silicate layers in the polymer matrix, electron tomography technique has been applied recently [7–11]. However, this technique is very time consuming and special care must be exercised during sample preparation. Furthermore, the analysis volume is substantially small and therefore, it is very difficult to get the global picture of clay particles distribution in the polymer matrix.

This article reports a new method for the 3D-analysis of silicate layers dispersion in the poly[(butylene succinate)-co-adipate] (PBSA) matrix using FIB-tomography technique.

* Fax: +27 12 841 2229.
E-mail address: rsuprakas@csir.co.za.

0032-3861/$ – see front matter © 2010 Elsevier Ltd. All rights reserved.
doi:10.1016/j.polymer.2010.06.025

a [-O-{$(CH_2)_4$-O}-{CO-$(CH_2)_2$-CO-}$_x$-{CO-$(CH_2)_4$-CO-}$_y$-]

x+y= 1

b

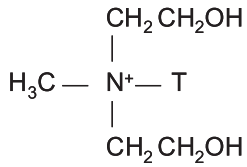

Fig. 1. (a) The molecular structure of poly[(butylene succinate)-co-adipate] and (b) chemical structure of bis(2-hydroxylethyl) quaternary ammonium used to modify pristine MMT. 'T' represents tallow (~65% C18; ~30% C16; ~5% C14).

2. Experimental part

2.1. Materials and composite preparation

PBSA is a synthetic aliphatic polyester and is synthesized by the polycondensation of butane-1,4-diol in the presence of succinic and adipic acids with relatively low production cost and satisfactory mechanical properties equivalent to that of polyolefins [12]. The PBSA, compared with poly(butylene succinate) (PBS), is more susceptible to degradation (both in compost and soil) because of its lower crystallinity and more flexible polymer chains [12]. It also has excellent processibility, so that it can be processed in the field of textiles into melt blow, multifilament, monofilament, flat, and split yarn, and also in the field of plastics into injection-moulded products. It is, thus, a promising polymer for various applications.

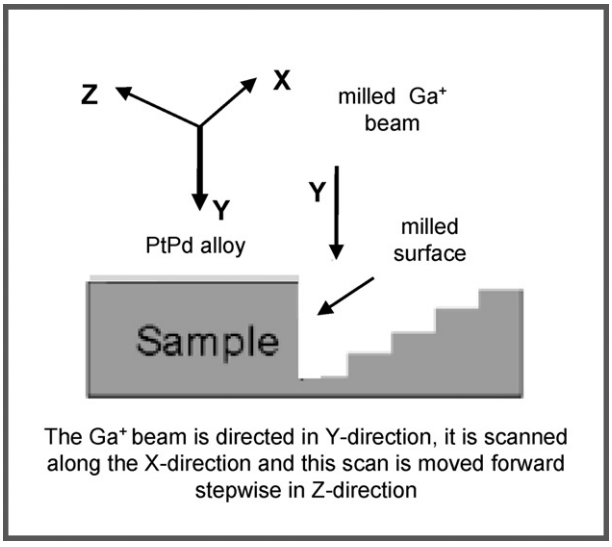

Fig. 2. Method of focused ion beam sectioning using Gallium ion perpendicular to the sample surface.

The PBSA used in this study is a commercial product from Showa High Polymer (Japan), with the designation BIONOLLE #3001, which according to the supplier has a weight average molecular weight, $M_w = 190$ kg/mol, density = 1.23 g/cm^3 (ASTM D-729), melt flow index (MFI) = 1.8 gm/10 min (190 °C, 2.16 kg, ASTM-1238), glass transition temperature, $T_g = -43.8$ °C, and melting temperatures, T_m's = 83.1 °C (first) and 94.5 °C (second). Here the reported results are from the second run. PBSA matrix generally shows two melting points and this is due to the presence of two different types

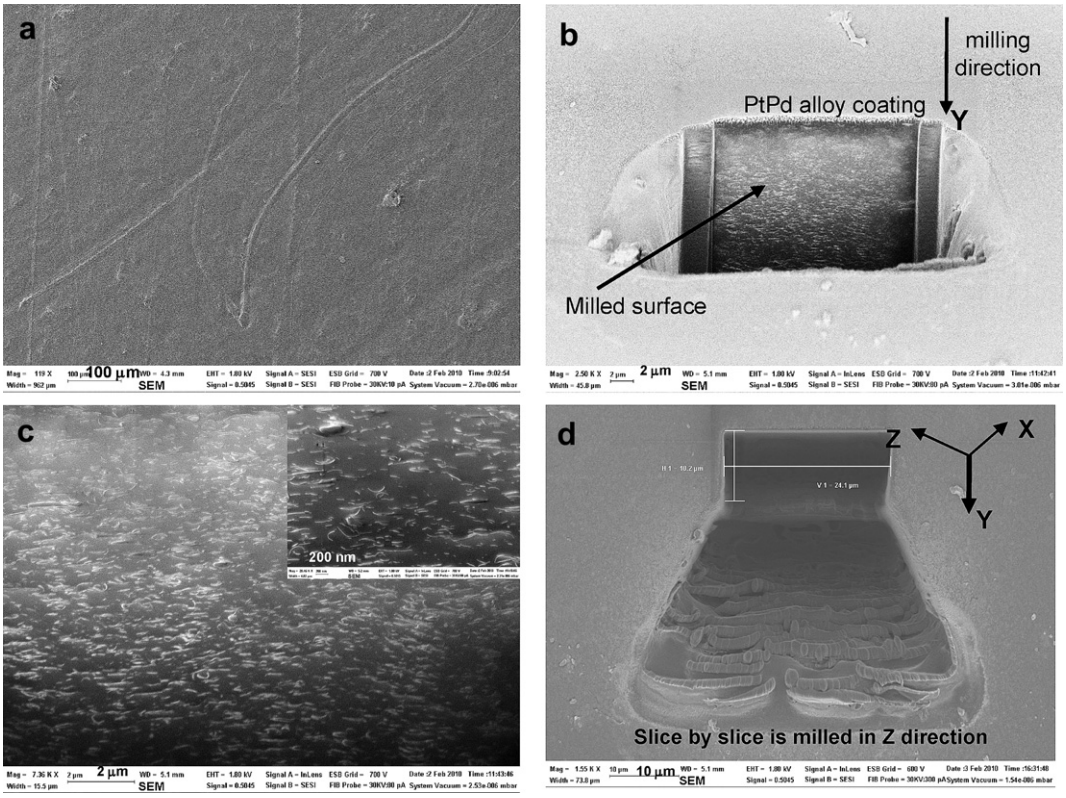

Fig. 3. (a) Scanning electron microscopy image of nanocomposite film surface without protective PtPd alloy, (b) imaging of milled surface using scanning electron microscopy where white lines are clay particles (cross-section perpendicular to the sample surface), (c) scanning electron microscopy images of polished surface where white lines are clay particles (inset high magnification image), and (d) sectioning nanocomposite film into many parallel two-dimensional slices (here 333 slices), which were used for 3D-reconstruction.

Table 1
Mechanical and material properties of PBSA and PBSACN.

Sample	Storage modulus at 25 °C[a]	Tensile properties[b]			O_2 gas permeability coefficient/ (ml mm/m^2 day MPa)[c]
		Modulus/MPa	Strength/MPa	Tenacity/%	
PBSA	0.52 GPa	213.2 ± 9	16.7 ± 0.8	440 ± 2	87
PBSACN	0.84 GPa	272.1 ± 15	20.0 ± 1	660 ± 5	29

[a] Average of three independent tests.
[b] Average of eight independent tests.
[c] Oxygen (O_2) gas transmission rate of neat PBSA and various PBSCN were measured at 25 °C and 90% relative humidity by the ASTM D-1434 differential pressure method (GTR-30XAU, Yanaco Co.). Test samples were prepared by compression moulding (thickness ~150 μm), and melt-quenched samples were used for this measurement. Reported results are average of three independent tests.

of crystals [13]. The molar ratio of succinate unit to the adipate unit is ~4:1 and the content of the coupling agent (hexamethylene diisocyanate) unit is ~0.5 mol%. Organoclay used in this study was Cloisite®30B (C30B), purchased from the Southern Clay Products, USA. According to the supplier, the pristine montmorillonite (MMT) is modified with 30 wt% of methyl tallow bis(2-hydroxylethyl) quaternary ammonium salt. The reason for choosing C30B as an organoclay in this study is that it has the closest value of the polar solubility parameter of the surfactant (21.5 $J^{1/2}/cm^{3/2}$) with that of PBSA (23.8 $J^{1/2}/cm^{3/2}$) [14]. Prior to melt-blending, the polymer was dried under vacuum at 60 °C for 48 h and C30B at 75 °C for 4 h. The molecular structures of PBSA and the surfactant used to modify pure MMT are, respectively, presented in parts (a) and (b) of Fig. 1.

Nanocomposite of PBSA (PBSACN) with C30B was prepared by melt-blending technique and the C30B content in the PBSACN was 3 wt%. PBSA was first melted in a Polylab Thermohaake-batch mixer (capacity = 50 g, counter rotating roller rotor 600, 557–1030) at 125 °C (set temperature) for 1.5 min with a rotor speed of 60 rpm. The C30B powder was added for 1 min and blended for 6.5 min. The dried PBSACN strands were then compression-moulded at 135 °C for 10 min to prepare a PBSACN film of ~160 μm thick and 200 mm wide, using Craver Laboratory compression moulder.

2.2. FIB-tomography

In recent years, FIB technique has become very popular mainly in semiconductor industry for a quick failure analysis at a high-resolution and mask repair. FIB technique is also becoming popular for the preparation of high-resolution TEM sample and cross-section analysis [15,16]. The 3D-tomography of a material using FIB/scanning electron microscopy (SEM) cross beam system starts by cutting 2D-slices through the selected volume by milling steps and cross-section can be imaged by high-resolution SEM (HR-SEM). Then the 2D-images are aligned using cross correlation of reference markers and finally, computer reconstruction of 2D-images enables the 3D-morphology of the dispersed silicate layers in the polymer matrix.

To have more homogeneous dispersion of silicate layers in the PBSA matrix, the middle portion of the compression-moulded film was used for FIB study (Zeiss FIB/SEM cross beam, model NVision 40). For the preparation of cross sections using FIB, the Gallium ion beam was perpendicular to the sectioning plane of interest as shown in Fig. 2. To avoid damage, prior to the milling, the PBSACN

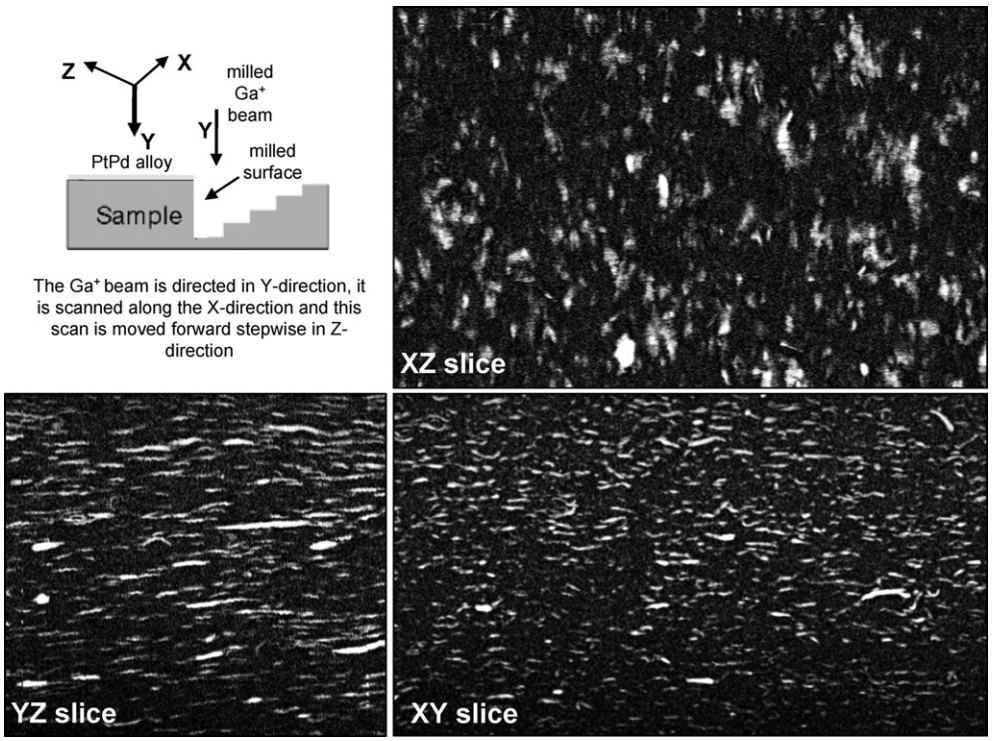

Fig. 4. Cross-sectional view of the nanocomposite sample, in which three digital slices from different planes are displayed. XY slice is one of the original SEM image, (Fig. 3c) while the XZ and YZ slices are virtual slices extracted digitally from the 3D-data set.

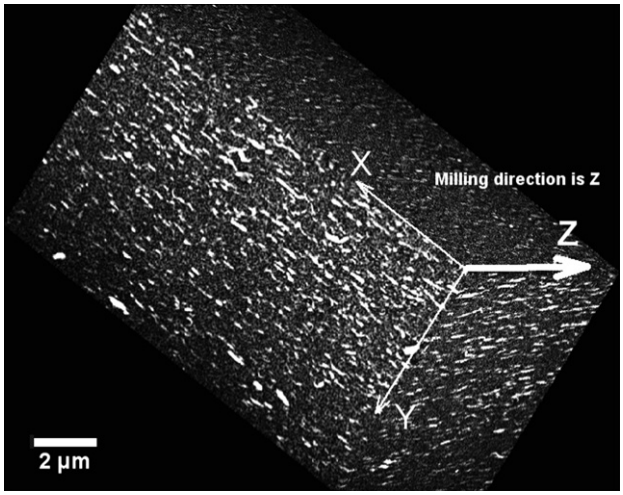

Fig. 5. 3D-representation of layered silicate dispersion (white parts) in PBSA matrix. The reconstructed volume after data processing was 14.85 × 8.55 × 9.51 μm^3. Milling direction is 'Z' refers to the direction of slicing.

film was sputter coated using PtPd alloy for 60 s at 40 mA current. At first, a deep 2D-cross-sectional surface through the sample was milled using a milling current of 13 nA. The cross-section was then polished by employing a milling current of 1.5 nA. After that, an appropriate ion beam current of 300 pA was selected to get a highly polished surface and high-resolution image, Fig. 3.

2.3. Fourier-transform infrared (FT-IR) spectroscopy

The interfacial interaction between PBSA matrix and C30B was studied by FT-IR spectroscopy, using a PerkinElmer Spectrum 100 spectrometer.

3. Results and discussion

The mechanical and material properties of pristine PBSA and PBSACN are presented in Table 1. It is clear from table that the properties of pure polymer concurrently improved after nanocomposite formation with 3 wt% C30B. Such improvements indicate the homogeneous dispersion of silicate layers in the matrix and intimate contact between dispersed particles, which is responsible for the effective transfer of load from matrix to filler and then filler to matrix. Therefore, to get information of dispersed layered silicates in real-space, FIB-tomography study of PBSACN was carried out.

Using FIB, about 333 slices of 24 × 12 × 10 μm^3 of volume were cut from PBSACN sample (refer Fig. 3(d)) and image of each slice was captured by HRSEM (1.8 kV, 30 μm aperture, HC mode, scan speed 8, inlens-SE detector, 1024 × 768 pixel, pixel size 15 nm). The thickness of each slice was 30 nm. 2D-images were then aligned using reference marker and 3D-reconstruction was done automatically using instrument software (Zeiss smart3D). Before reconstruction process starts voxel size was corrected in the vertical axis since images are normally tilted about 52°. The reconstructed volume after data processing was 14.85 × 8.55 × 9.51 μm^3. Fig. 4 shows the dispersion of silicate layers in different planes. From the elemental analysis using X-ray (EDS analysis), Si, Al, Mg, and oxygen were mainly identified and from the elemental compositional analysis, the white particles were found to be MMT, used for the preparation of PBSACN. It is clear from the images that silicate particles have platelet like geometry, mostly intercalated, nicely oriented (particularly in the YZ- and XY-planes), and finely dispersed in the PBSA matrix. Moreover, the intercalated particles are mostly interconnected, forming network like geometry inside the PBSA matrix.

Fig. 5 shows a reconstructed 3D-volume of layered silicate particles (PBSA is transparent). It is clear from the reconstruction that the layered silicate particles are completely embedded within the PBSA matrix and forming an interconnected network like structure. This information is very crucial in understanding the overall integrity of the PBSACN and predicting its mechanical and other properties. It is interesting to note that the tomography results are supporting our previous conclusion based on small-angle X-ray scattering results, silicate layers possess the thickness in a range of 4.5–7.5 nm and they are overlapping each other [17].

We believe this interconnected network is responsible for the effective transfer of load and improved mechanical properties of PBSACN (refer Table 1). The parallel arrangement of silicate particles in the YZ/XY-planes is responsible for the significantly improved oxygen gas barrier property of PBSACN by creating a long "tortuous path" that slowing down the progress of gas molecules through the matrix resin. This interconnected superstructure is also responsible for the decrease in degree of crystallinity of PBSA matrix in the case of PBSACN by acting as obstacles for the mobility and flexibility of the PBSA chains to fold and join the crystallization growth front [18]. This actually hindering the local lamellar crystallization and leads to the decrease matrix crystallinity. The degree of crystallinity decreased from ~48% for pristine PBSA to ~42% for PBSACN [13,19].

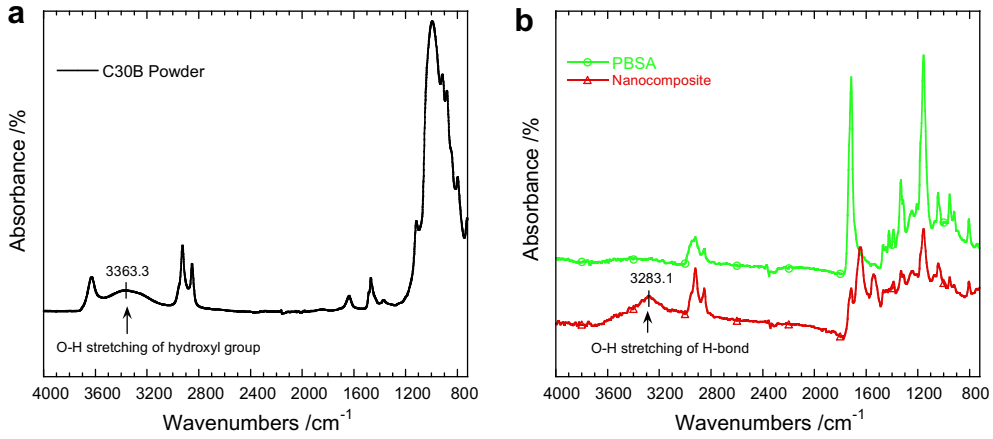

Fig. 6. FT-IR spectra of C30B powder, pristine PBSA matrix, and PBSA/C30B nanocomposite containing 3 wt% C30B. Results show the formation of hydrogen bonding between 'CO' groups on the PBSA backbone and hydroxyl groups present in the C30B.

Now the question is – what is the main driving force for the homogeneous dispersion of silicate layers in the PBSA matrix. As we mentioned before the reason for choosing C30B as an organoclay for the preparation of composite with PBSA is that it has the closest value of the polar solubility parameter of the surfactant with that of PBSA. To find out the presence of interfacial interactions between the matrix and C30B particles, FT-IR spectroscopic analysis (using attenuated total reflection IR imaging technique) of pure C30B powder, pure PBSA matrix, and their nanocomposite were carried out, and results are presented in Fig. 6. The analysis of FT-IR spectra of C30B, PBSA, and PBSACN [20], indicates the presence of strong interactions between the C30B particles and PBSA matrix, which eventually leads to the formation of hydrogen bonding between 'CO' groups on the PBSA backbone and hydroxyl groups present in the C30B. The formation of hydrogen bonding is responsible for the high degree of confinement of polymer chains inside the silicate layers and hence, homogeneous dispersion of intercalated silicate layers in the PBSA matrix.

4. Conclusions

This study shows that FIB-tomography is a powerfull technique to characterize the real-space distribution of layered silicate particles in the polymer matrix. This information is very crucial in understanding the overall integrity of the nanocomposite and to correlate the dispersed morphology of the silicate layers with the macroscopic performance of the nanocomposite materials, which helps in designing of nanocomposite materials with desired properties.

Acknowledgements

Author acknowledges the financial support from the CSIR Executive and the Department of Science and Technology, South Africa. Author would also like to express his appreciation to Ms J. Bandyopadhyay for FT-IR studies and Dr. Heiko from Zeiss for FIB-studies.

References

[1] Pavlidou S, Papaspyrides CD. A review on polymer-layered silicate nanocomposites. Prog Polym Sci 2008;33:1119–98.
[2] Fernandez-Saavedra R, Darder M, Gomez-Aviles A, Aranda P, Ruiz-Hitzky E. Polymer-clay nanocomposites as precursors of nanostructured carbon materials for electrochemical devices: templating effect of clays. J Nanosci Nanotechnol 2008;8:1741–50.
[3] (a) Sinha Ray S, Bousmina M. Biodegradable polymers and their layered silicate nanocomposites: in greening the 21st century materials world. Prog Mater Sci 2005;50:962–1079;
(b) Sinha Ray S, Okamoto M. Polymer/layered silicate nanocomposites: a review from preparation to processing. Prog Polym Sci 2003;28:1539–641.
[4] Alexandre M, Dubois P. Polymer-layered silicate nanocomposites: preparation, properties, and uses of a new class of materials. Mater Sci Eng 2000; R28:1–63.
[5] Morgan AB, Gilman JW. Characterization of poly-layered silicate (clay) nanocomposites by transmission electron microscopy and X-ray diffraction: a comparative study. J Appl Polym Sci 2003;87:1329–38.
[6] Drummy LF, Koerner H, Farmer BL, Vaia RA. In: Carrado Kathleen A, Bergaya Faiza, editors. CMS Workshop Lectures, vol. 15. Virginia: The Clay Minerals Society; 2007. p. 97.
[7] Sinha Ray S. Visualisation of nanoclay dispersion in polymer matrix by high-resolution electron microscopy combined with electron tomography. Macromol Mater Eng 2009;294:281–6.
[8] Yoonessi M, Toghiani H, Daulton TL, Lin JS, Pittman Jr UC. Clay delamination in clay/poly(dicyclopentadiene) nanocomposites quantified by small angle neutron scattering and high-resolution transmission electron microscopy. Macromolecules 2005;38:818–38.
[9] Yaroon-Marcovich D, Chen Y, Nir S, Prost R. High resolution electron microscopy structural studies of organo-clay nanocomposites. Environ Sci Technol 2005;39:1231–8.
[10] Jinnai H, Shinbori Y, Kitaoka T, Akutagawa K, Mashita N, Nishi T. Three-dimensional structure of a nanocomposite material consisting of two kinds of nanofillers and rubbery matrix studied by transmission electron microtomography. Macromolecules 2007;40:6758–64.
[11] Drummy LF, Wang YC, Schoenmakers R, May K, Jackson M, Koerner H, et al. Morphology of layered Silicate–(nanoclay–) polymer nanocomposites by electron tomography and small-angle X-ray scattering. Macromolecules 2008;41:2135–43.
[12] Ishioka D. Biopolymers, polyesters III. Applications and commercial products, vol. 4. Weinheim: Wiley-VCH Verlag Gmbh; 2002. p. 275.
[13] Bandyopadhyay J, Maity A, Khatua BB, Sinha Ray S. Thermal and rheological properties of biodegradable poly[(butylene succinate)-co-adipate] nanocomposites. J Nanosci Nanotechnol 2010;10:4184–95.
[14] Krevelen DWV. Properties of polymers. Amsterdam, The Netherlands: Elsevier; 1990.
[15] Lasagni FL, Lasagni A, Engstler M, Degischer HP, Mucklich F. Nano-characterization of cast structures by FIB-tomography. Adv Eng Mater 2008;10:62–6.
[16] McGrouther D, Munroe PR. Imaging and analysis of 3-D structure using a dual beam FIB. Micros Res Tech 2007;70:186–94.
[17] Bandyopadhyay J, Sinha Ray S. The quantitative analysis of nano-clay dispersion in polymer nanocomposites by small angle X-ray scattering combined with electron microscopy. Polymer 2010;41:1437–49.
[18] Sinha Ray S, Bousmina M. Structure and properties of nanocomposites based on poly(butylene succinate-co-adipate) and organically modified montmorillonite. Macromol Mater Eng 2005;290:759–68.
[19] Sinha Ray S, Bousmina M. Crystallization behavior of poly[(butylene succinate)-co-adipate] nanocomposite. Macromol Chem Phys 2006;207: 1207–19.
[20] Socrates G. Infrared and Raman characteristic group frequencies. 3rd ed. New York: John Wiley and Sons, Ltd; 2001.